RSC Advances

PAPER

View Article Online
View Journal | View Issue

Cite this: *RSC Adv.*, 2026, **16**, 22440

Comprehensive study of tunable BiOI/BiOBr heterojunctions: reactive species and mechanistic insights for visible-light degradation of indigo carmine

Cheewita Suwanchawalit,[a] Soontorn Suvokhiaw,[a] Montri Aiempanakit,[b] Hoang-Vinh-Truong Phan,[cd] Van-Kieu Nguyen[ef] and Le-Thuy-Thuy-Trang Hoang *[gh]

In recent years, heterojunction composites of bismuth-based oxyhalides (BiOX, X = F/Cl/Br/I) have emerged as effective visible-light-driven photocatalysts. Despite notable advances, particularly the promising performances of bulk BiOI/BiOBr in degrading methyl orange and the synergistic effects observed in their thin films for indigo carmine (IC) photodegradation, key gaps still persist. These include the lack of a comprehensive investigation into simple, tunable bulk BiOI/BiOBr heterojunctions and the insufficient elucidation of reactive species for charge-transfer mechanisms governing dye remediation. This study introduces a facile and scalable approach for synthesizing bulk BiOI/BiOBr heterostructures *via* a modified deposition–precipitation method, offering an efficient alternative to complex thin-film systems and providing the first comprehensive characterization, mechanistic insight, and reactive species identification into IC degradation over bulk BiOI/BiOBr composites. Evaluation of their photocatalytic activity towards IC degradation under 4-hour visible light irradiation demonstrated 0.6BiOI/0.4BiOBr with the best performance of over 90% degradation efficiency, attributed not only to the improved light absorption but also to the effective separation of photogenerated charge carriers across the heterojunction interface. Radical scavenging experiments revealed that superoxide radicals ($^{\bullet}O_2^-$) and photogenerated holes (h^+) are the dominant reactive species, while the band structure analysis suggested that the generation of $^{\bullet}O_2^-$ cannot be fully explained by a conventional band-to-band mechanism, implying a defect-assisted interfacial charge transfer pathway for O_2 activation. These findings not only establish bulk BiOI/BiOBr as a promising, scalable photocatalyst for wastewater treatment but also provide improved insight into heterojunction-mediated charge separation and defect-assisted processes governing IC degradation under visible light.

Received 17th March 2026
Accepted 23rd April 2026

DOI: 10.1039/d6ra02228f

rsc.li/rsc-advances

1. Introduction

For years, dyes, either natural or synthetic, have been essential materials in the development of printing, leather, tannery, textile, paint, plastic, rubber, or cosmetics industries.[1–3] Notably, indigo carmine (IC) is one of the most common dyestuffs which was widely applied in pharmaceutical, cosmetics, food, and textile denim dyeing industries[4–6] with nearly 40 thousand tons are annually manufactured.[7] However, the extensive production and application of IC dyes have generated and discharged a substantial amount of hazardous dyes liquor into aqueous environment.[3] The dissemination of wasted IC dyes in water sources can detrimentally affect the balance of aquatic ecology,[8] while direct contact to water contaminated by IC dyes can result in severe human health concerns, such as damaging conjunctiva and cornea,[9,10] harmful effects on respiratory tract, or severe skin irritation.[10,11]

[a]*Department of Chemistry, Faculty of Science, Silpakorn University, Nakhon Pathom, 73000, Thailand*
[b]*Department of Physics, Faculty of Science, Silpakorn University, Nakhon Pathom, 73000, Thailand*
[c]*Institute of Fundamental and Applied Sciences, Duy Tan University, Ho Chi Minh City 700000, Vietnam*
[d]*Faculty of Natural Sciences, Duy Tan University, Da Nang 550000, Vietnam*
[e]*Center for Hi-Tech Development, Nguyen Tat Thanh University, Saigon Hi-Tech Park, Ho Chi Minh City, Vietnam*
[f]*Institute of Interdisciplinary Sciences (IIS), Nguyen Tat Thanh University, Ho Chi Minh City, Vietnam*
[g]*Institute of Applied Science and Technology, Van Lang School of Technology, Van Lang University, Ho Chi Minh City, Vietnam. E-mail: trang.hltt@vlu.edu.vn*
[h]*Faculty of Applied Technology, Van Lang School of Technology, Van Lang University, Ho Chi Minh City, Vietnam*

Therefore, the removal of IC dyes from the wastewater of dye-consuming industries has become of great interest among scientists, approaching adsorption, ultrafiltration, electrocoagulation, electrodialysis, chemical oxidation, bacterial treatment, micellar catalysis, photolysis, and especially photocatalytic degradation, as feasible methods.[10]

As an advanced oxidation process,[3] photocatalytic degradation involves the application of a photocatalyst whose activation under light *via* photon adsorption can accelerate chemical transformation.[3,12] In environmental remediation, this light-driven catalytic oxidation has been considered as an eco-friendly and economical approach to eradicate organic and inorganic pollutants,[13] specifically in IC dyes removal.[3] Accordingly, the effectiveness of TiO_2 as a semiconductor photocatalyst for the photodegradation of IC has been acknowledged.[14] However, due to the large band gap energy (E_g) of 3.0–3.2 eV,[15] TiO_2 can only exhibit prominent photocatalytic effects under expensive and harmful ultraviolet (UV) illumination[16] which limited the material efficiency in utilizing solar energy.[17] This drawback has proposed the tendency in developing novel photocatalysts with narrower E_g and more efficient visible-light response,[16] accounting for 47% of the solar spectrum.[17]

Bismuth-based oxyhalides (BiOX, X = F, Cl, Br, I) are recently targeted as potential light active photocatalysts whose significant photocatalytic activity was due to the good electrical/optical properties,[13,15] and the characteristic layered structure containing a $[Bi_2O_2]^{2+}$ layer and double halogen ions.[18] In comparison with other bismuth-based oxyhalides,[17] the lowest E_g of 1.7–1.83 eV makes BiOI the most potential visible light responsive photocatalyst.[15] Although the photodegradation of various dyes such as rhodamine B,[19] methyl orange,[20] and IC[16] with BiOI as photocatalysts have been reported, its photocatalytic activities are till limited by the fast recombination of its photogenerated electron and hole (e^-/h^+) pairs.[13] Recently, the development of materials with heterojunction structure has been regarded as one of the most promising strategies to enhance the effectiveness of a photocatalyst.[21,22] In this context, different BiOI-based composite photocatalysts prepared by constructing the heterojunctions between BiOI and other metal semiconductors have been developed[23–27] to suppress the material's e^-/h^+ recombination process[13] and enhance the photocatalytic activity. Notably, the combination of BiOI with other bismuth-based oxyhalides, particularly BiOBr was considered as the most advantageous approach as their similarity in the valence state with halogens of the same properties, and the layered and matched lattice structures can facilitate the separation of electron hole (e^-/h^+) pairs.[18] Accordingly, the more significant photodegradation efficiencies of bulk BiOI/BiOBr catalytic composites for methyl orange[15] and heterojunction films of BiOI and BiOBr for IC[28] were reported. The thin-film studies have demonstrated promising synergistic effects between BiOI and BiOBr, however, they are constrained by the technical challenges associated with synthesis, which limit their scalability for practical IC dye remediation. In contrast, bulk materials offer a viable alternative to these challenging thin-film configurations. Unfortunately, most previous studies on bulk BiOI/BiOBr composites lacked in-depth X-ray photoelectron spectroscopy (XPS) analysis for elemental composition and radical trapping experiments for reactive species identification, underscoring the need for a more comprehensive study to fully elucidate the mechanistic aspects of IC dye degradation. This gap is further emphasized by the limited applicability of existing work specifically addressing IC degradation.

The present study addresses these shortcomings through a simplified synthesis route for bulk, tunable BiOI/BiOBr composites with controllable phase composition and interface structure. Comprehensive characterization of the as-prepared photocatalysts was carried out using X-ray powder diffraction (XRD), field emission scanning electron microscopy (FE-SEM), energy dispersive X-ray spectroscopy (EDX), Fourier transform infrared spectroscopy (FTIR), ultraviolet-visible diffuse reflectance spectroscopy (UV-vis DRS), ultraviolet-visible spectrophotometry, X-ray photoelectron spectroscopy (XPS), and fluorescence spectroscopy. Furthermore, the effects of the BiOI to BiOBr ratio on the composites' photocatalytic performance and the possible degradation mechanism were systematically investigated. By providing a holistic analysis – including advanced characterization of structure and composition, reactive species trapping experiments, and a proposed charge-transfer mechanism, this work bridges the existing knowledge gap in understanding IC dye photodegradation pathways, offering valuable insights for designing efficient and scalable photocatalytic systems for environmental remediation.

2. Experimental

2.1. Materials

All the reagents, including bismuth(III) nitrate pentahydrate ($Bi(NO_3)_3 \cdot 5H_2O$) (KemAus, Australia), potassium iodide (KI) (Carlo Erba, Italy), potassium bromide (KBr) (Fluka, USA), sodium hydroxide (NaOH) (Loba Chemie Pvt. Ltd, India), nitric acid 70% (HNO_3) (Carlo Erba, Italy), indigo carmine (Sigma-Aldrich, USA), *tert*-butyl alcohol (*t*-butanol) (Fluka, USA), ethylene diamine tetraacetic acid (EDTA) (Fluka, USA), *p*-benzoquinone (Acros Organics B.V.B.A., Belgium), were purchased and used as received without purification. Distilled water was used throughout the experiment.

2.2. Preparation of bismuth oxyhalides BiOI and BiOBr

In 20 mL of 2 M HNO_3, 0.48507 g (1 mmol) of $Bi(NO_3)_3 \cdot 5H_2O$ was dissolved to prepare a $Bi(NO_3)_3$ solution, to which KI (0.332 g – 2 mmol, dissolved in 20 mL of distilled water) or KBr (0.238 g – 2 mmol, dissolved in 20 mL of distilled water) solutions were slowly and dropwise added during agitation. The solution's pH was then adjusted to 10, followed by continuous agitation at room temperature for an hour. Subsequently, the resulting precipitates were filtered by a vacuum filtration system with 0.1-micron filter paper, washed with distilled water, and dried at 70 °C for 12 hours.

2.3. Preparation of BiOI/BiOBr heterojunction photocatalysts

The synthesis of BiOI/BiOBr composites was accomplished *via* a modified deposition–precipitation method, and the procedure was described as follows. At first, a $Bi(NO_3)_3$ solution was prepared by dissolving 0.48507 g of $Bi(NO_3)_3 \cdot 5H_2O$ in 20 mL of 2 M HNO_3 (solution A). Then another solution containing KI and KBr mixture at varying mmol ratios of 0.8 : 0.2, 0.6 : 0.4, 0.4 : 0.6, and 0.2 : 0.8 was prepared in 20 mL of distilled water (solution B). Subsequently, solution B was added to solution A drop by drop with stirring till they were fully incorporated, and the final solution was adjusted to pH 10.0 using 2 M NaOH. The reaction was conducted at room temperature for an hour with continuous agitation. Later on, the synthesized precipitate was filtered by a vacuum filtration system with a 0.1-micron filter paper, washed with distilled water, and dried at 70 °C for 12 hours to obtain the required composites.

2.4. Material characterization

XRD patterns of the synthesized materials were obtained by a LabX XRD-6100 X-ray diffractometer (Shimadzu, Japan) operated over a 2θ range of 5 – 70° with Cu Kα radiation (40 kV, 8 mA) and a scanning speed of 2° per minute. FE-SEM images on Tescan Mira3 (Czech Republic), equipped with an EDX spectrometer (Ametek Edax), was utilized to explore the surface morphology and the elemental mapping of the synthesized materials, while their molecular structures were examined *via* FT-IR spectra over the wavenumber range 4000–400 cm^{-1}, provided by a spotlight 200i FT-IR microscope (PerkinElmer, USA). UV-vis DRS analysis and fluorescence spectral measurement with an excitation wavelength of 370 nm were conducted by a UV 2600i spectrophotometer (Shimadzu, Japan) and a LS-55 spectrometer (PerkinElmer, USA), respectively. The XPS analysis was conducted by a Kratos Axis Ultra spectrometer and a monochromatic Al Kα source at 1486.7 eV.

2.5. Photocatalytic degradation experiments

The degradation of IC dye under visible light exposure using BiOI, BiOBr, and the prepared composites was examined to evaluate their photocatalytic activities, and was detailed as follows. To a beaker containing 50 mL of IC solution (5×10^{-5} M), 0.05 g of the synthesized catalyst was added. The suspension was placed in a dark chamber and stirred for 30 minutes to initiate an adsorption–desorption equilibrium between the synthesized photocatalysts and IC dye before being exposed to visible light, provided by two 18 W daylight lamps (Philips TL-D 18 W/865 without UV filter), under magnetic agitation. After specific time intervals of 1, 2, 3, and 4 hours, 5 mL of the corresponding IC solutions was collected, centrifuged, and analyzed using a Lambda 35 UV/vis spectrometer (PerkinElmer, USA) over a wavelength range of 400–700 nm to reveal the decrease in IC concentration, whose absorbance was recorded at 610 nm. Accordingly, the percentage of IC degradation was calculated using eqn (1), in which A_0 is the initial absorbance of IC, and A_t is its absorbance at a specific time.

$$\%\text{Degradation} = \frac{(A_0 - A_t)}{A_0} \times 100 \quad (1)$$

2.6. Scavenger experiments

In order to identify the relevant reactive species throughout the photodegradation of IC catalyzed by BiOI/BiOBr composites, the addition of particular scavengers, namely benzoquinone (BQ), ethylenediaminetetraacetic acid (EDTA) and *t*-butanol, trapping superoxide radicals ($^{\bullet}O_2^-$), h^+, and $^{\bullet}OH$, respectively, was carried out during the photocatalytic degradation process. Accordingly, to a series of four 50 mL beakers containing solutions of 0.05 g catalyst and 5×10^{-5} M IC solution, 5 mL of distilled water, BQ (0.001 M), EDTA (0.01 M), and *t*-butanol (0.01 M) were respectively added. Each solution was put into a dark chamber with stirring for 30 minutes, followed by 4-hour exposure under visible light. For each hour interval, 5 mL of the IC solution was obtained, centrifuged, and introduced to a Lambda 35 UV/vis spectrometer (PerkinElmer, USA) to the determine the absorbance at 610 nm. Finally, the corresponding percentage of IC degradation was calculated using eqn (1).

3. Results and discussion

3.1. Characterization of the synthesized BiOI/BiOBr composites

BiOI, BiOBr, and their composites were all prepared as powder with a fine texture. XRD analysis of these materials was conducted to reveal their crystal structure. From the patterns given in Fig. 1, narrow and well-defined characteristic diffraction peaks at 29.21, 31.65, 45.27, 55.17, well indexed to the tetragonal BiOI (JCPDS-no. 10-0445), and at 10.45, 23.92, 25.34, 31.42, 39.24, 57.2, corresponding to the tetragonal BiOBr (JCPDS-no. 09-0393), were presented. These data were similar to those reported by Cao *et al.*[15] and Chowdhury and Shambharkar,[12] respectively, and thereby indicating the preparation of well crystallized BiOI/BiOBr composites. However, the intensities

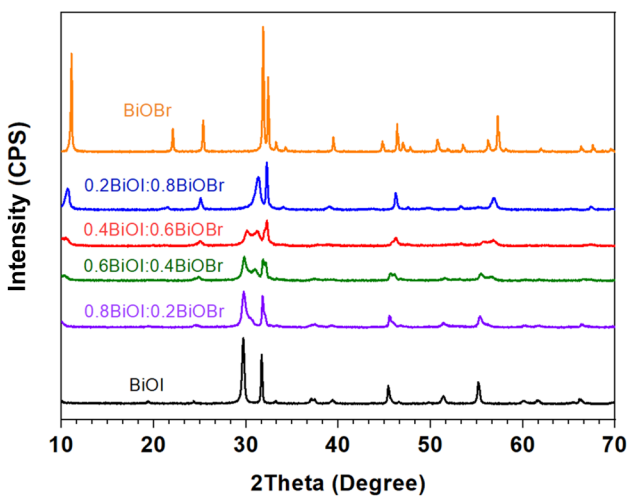

Fig. 1 XRD patterns of the synthesized materials.

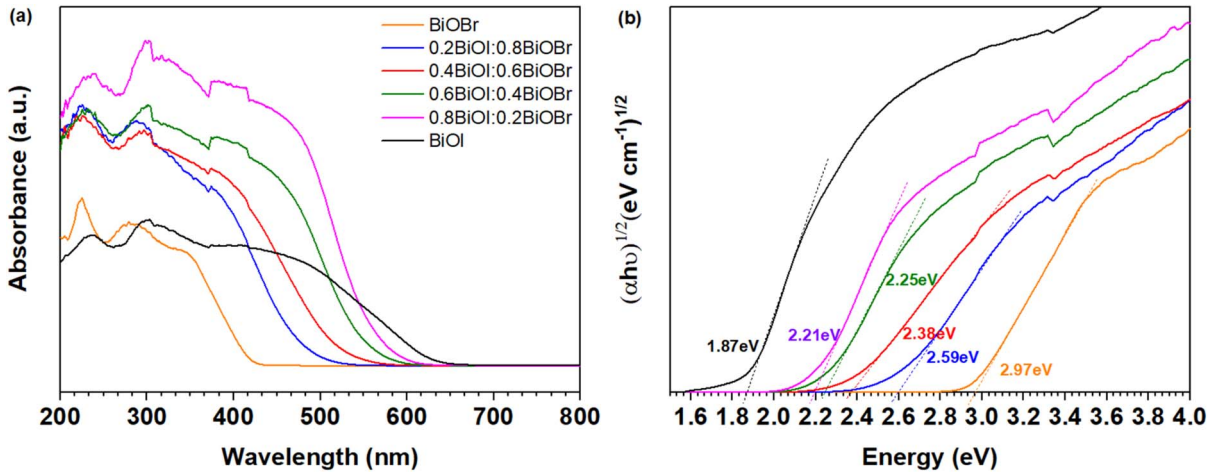

Fig. 2 UV-vis DRS spectra (a) and plots of $(\alpha h\gamma)^{1/2}$ *vs.* photon energy (b) of the synthesized materials.

and appearances of these peaks were observed with significant differences among the composites as the superior of those assigned to BiOI or BiOBr to another aligned with the respective KI/KBr ratios for their synthesis. Further analysis of the light adsorption range of the synthesized materials *via* UV-vis DRS also shared the similar manner. As for BiOI and BiOBr, it can be concluded from Fig. 2a that BiOI provided the more significant optical property at the wavelength shorter than 660 nm, while BiOBr was found with a narrower range of visible light absorption, displaying the maximum absorption edge at approximately 455 nm. Accordingly, regarding BiOI/BiOBr composites, as the BiOI amounts increased, the monotonic red shift of their absorption edges closer to that of BiOI occurred (Fig. 2a). Consequently, this led to the downward slope in the E_g of the prepared composites from 2.59 to 2.21 eV (Fig. 2b) which was mainly attributed to the strong visible light response of BiOI (E_g = 1.87 eV), and therefore making these composites more responsive to visible light than BiOBr (E_g = 2.97 eV).

As depicted from the 10 000×-magnified SEM images of the synthesized materials (Fig. 3), the morphological analysis revealed BiOI, BiOBr, and their composites to possess small and sheetlike structures. Extensive analysis further displayed the overlapping and aggregation of the composites's folded-sheet

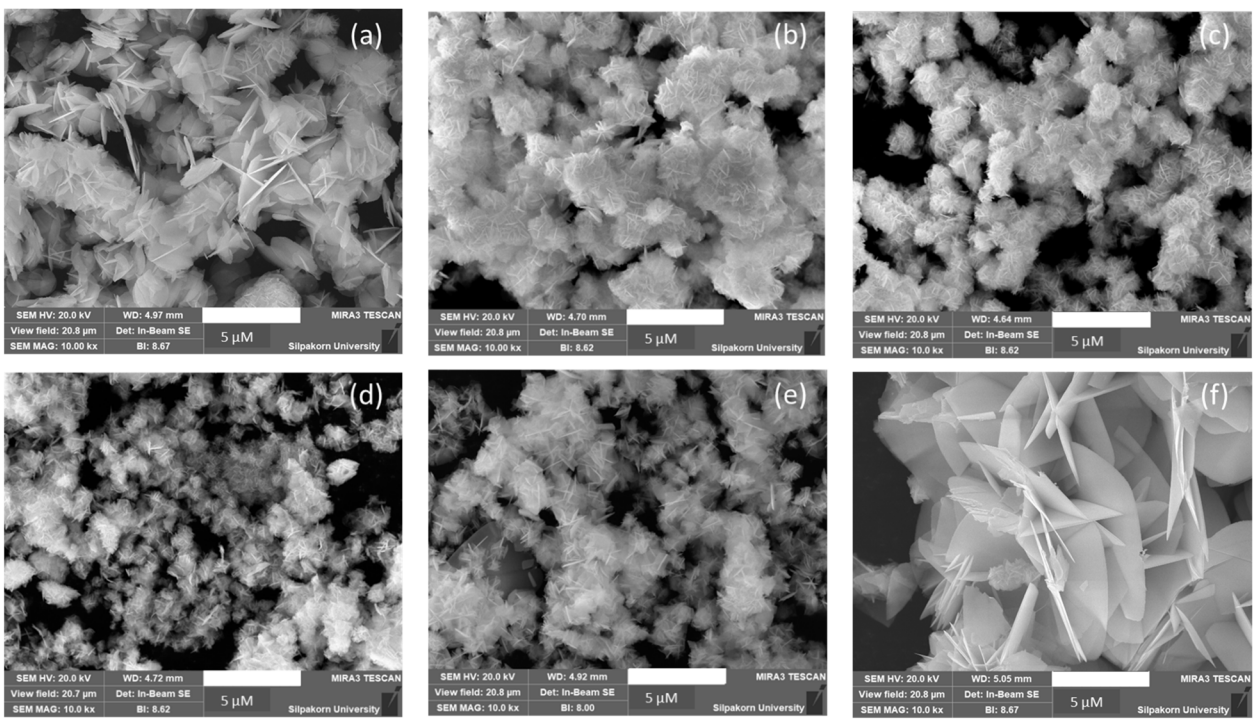

Fig. 3 SEM images of the synthesized materials: (a) BiOI; (b) 0.8BiOI/0.2BiOBr; (c) 0.6BiOI/0.4BiOBr; (d) 0.4BiOI/0.6BiOBr; (e) 0.2BiOI/0.8BiOBr; (f) BiOBr.

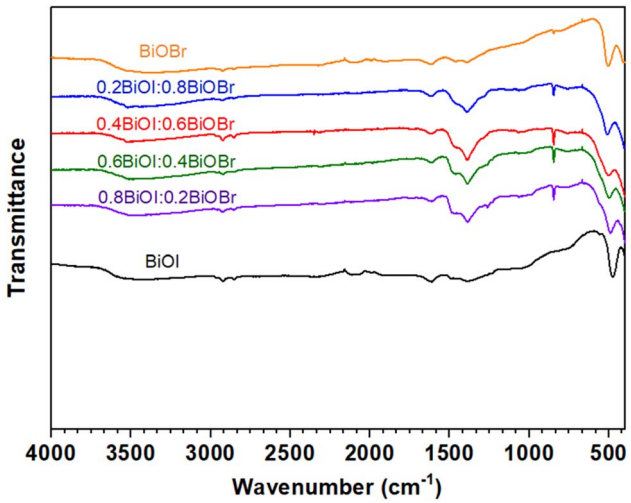

Fig. 4 FT-IR spectra of the synthesized materials.

structures into larger clusters with rougher and more irregular surface than those of the initial BiOI and BiOBr, Analyzing the FT-IR spectra of the as-prepared BiOI, BiOBr, and BiOI/BiOBr composites (Fig. 4) provided valid data on their surface functional groups. Accordingly, the identical vibration peaks located at around 3546–3407 cm^{-1} and 1605–1601 cm^{-1}, respectively assigned to O–H stretching vibration of absorbed water molecules and the O–H bending vibration of the interlayer OH groups,[29,30] and at 512–478 cm^{-1} and 846–844 cm^{-1}, respectively corresponding to Bi–O symmetric and asymmetric stretching vibrations,[30,31] were detected in all materials. Notably, the adsorption region in the range of 1500–1000 cm^{-1} with characterizing strong sharp peaks for Bi–I and Bi–Br bands in BiOI and BiOBr,[31,32] was found for all the composites.

In order to explore the compositional data of the synthesized composites, 0.6BiOI/0.4BiOBr composite was representatively examined *via* EDX and XPS analyses. It should be noticed that a certain amount of C detected in the elemental composition of the sample was attributed to the carbon tape used in preparing sample for EDX or the adventitious carbon from XPS instruments.[33] Accordingly, Fig. 5 provided the EDX spectrum with the strong O, I, Br, Bi peaks, and hence consolidating the existence of these elements in the analyzed composite, whose oxidation states on the surface were further verified by XPS analysis. As described in Fig. 6a, besides the identical appearances of O (at 530.1 eV) and Bi (at 161.9 eV) element peaks,[18,34,35] the wide XPS spectra of 0.6BiOI/0.4BiOBr composite also displayed those for both I (at 631.9 and 619.7 eV) and Br (at 68.7 eV) elements,[18] and therefore further confirming the compositional presence of these major elements, accounting for 33.17%, 26.04%, 10.64%, and 5.25% of elemental composition, respectively. The extensive analysis of high resolution XPS spectra of Bi 4f, O 1s, I 3d, and Br 3d were performed to emphasize the atomic valence within the composite's structure. From Fig. 6b, XPS spectrum of O 1s was dominated by the absorption peaks at 533.6, 531.4, and 530.1 eV, respectively assigned to the surface hydroxyl groups,[33] oxygen vacancies (I–O or Br–O),[18] and the lattice oxygen (Bi–O).[35] As for XPS spectrum of Bi 4f (Fig. 6c), the extensive absorption peaks of Bi $4f\frac{7}{2}$ and Bi $4f\frac{5}{2}$ with the binding energies of 159.2 and 164.5 eV, respectively, were shown, indicating the presence of typical Bi^{3+} in the composite.[33,35,36] Further analysis of XPS spectra of I 3d (Fig. 6d) and Br 3d (Fig. 6e) identified the respective pairs of characteristic peaks at 619.1–631.3 eV (for I $3d\frac{5}{2}$ and I $3d\frac{3}{2}$), and 68.2–69.7 eV (for Br $3d\frac{5}{2}$ and Br $3d\frac{3}{2}$), attributed to the -1-valence state of I and Br in the composite.[33,36,37] Interestingly, the slight alteration in the positions of Bi 4f, I 3d, and Br 3d peaks to the lower binding energy of 0.6BiOI/0.4BiOBr composite in comparison with the initial BiOI and BiOBr was in agreement with the report of Gao *et al.*[37] on the BiOBr/BiOI/Bi composite, indicating the close interactions between BiOI and BiOBr in the analyzed composite. These data, together with those previously

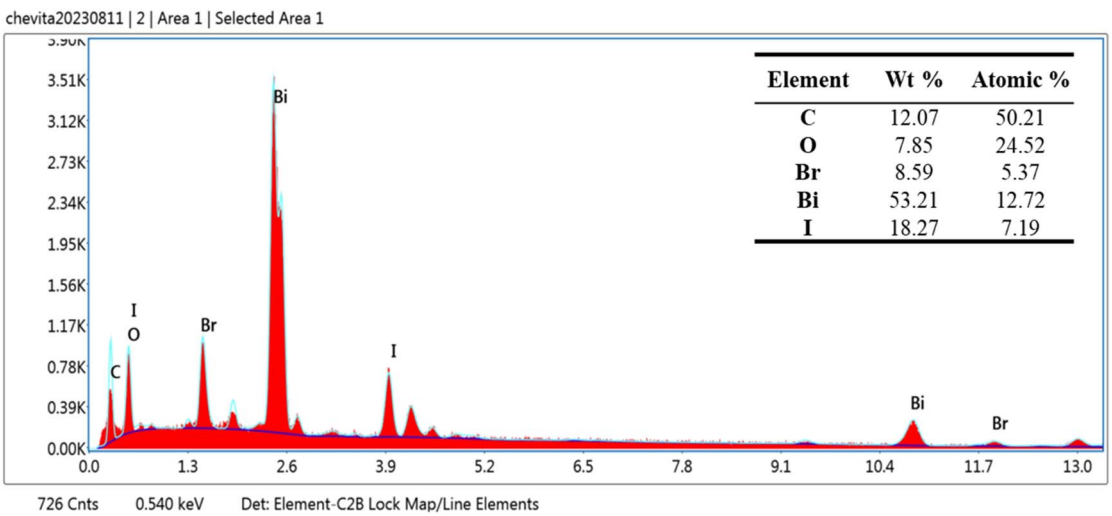

Element	Wt %	Atomic %
C	12.07	50.21
O	7.85	24.52
Br	8.59	5.37
Bi	53.21	12.72
I	18.27	7.19

Fig. 5 EDX spectrum of 0.6BiOI/0.4BiOBr composite.

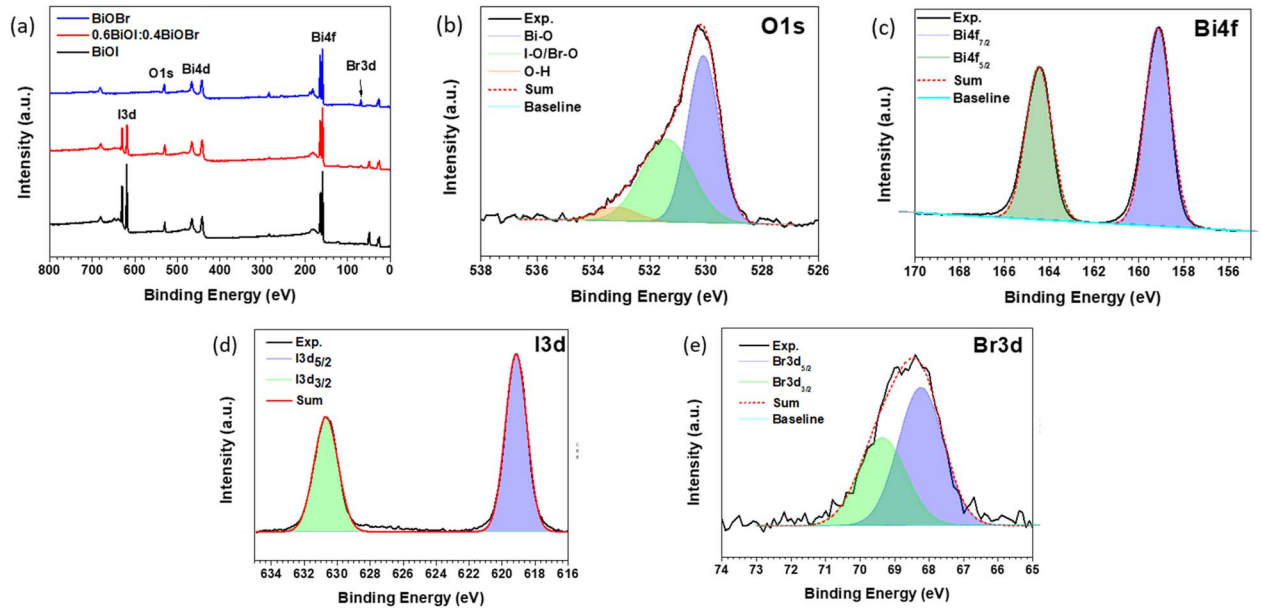

Fig. 6 The wide XPS spectra of BiOI, BiOBr, and 0.6BiOI/0.4BiOBr composite (a); the high resolution XPS spectra of O 1s (b), Bi 4f (c), I 3d (d), and Br 3d (e) for 0.6BiOI/0.4BiOBr composite.

discussed, consolidated the successful synthesis of the BiOI/BiOBr composites.

3.2. Photocatalytic degradation of IC dye using the synthesized BiOI/BiOBr composites

The performances of the as-synthesized materials in IC dye photodegradation were illustrated in Fig. 7. As the suspension was irradiated by visible light, the IC photodegradation was achieved under the photocatalytic activity of all the materials. Within the same time interval, all the prepared BiOI/BiOBr composites displayed the superior percentage of IC degradation at over 80% to both BiOI (around 60%) and BiOBr (around 10%). The enhanced photocatalytic activity of the composites, compared to the pristine BiOI and BiOBr, can be well explained *via* their photoluminescence (PL) spectra (Fig. 8). In comparison with pure BiOI and BiOBr, all the prepared BiOI/BiOBr composites exhibited significantly lower relative PL intensities, with 0.6BiOI/0.4BiOBr showing the weakest emission. This suggests a more efficient suppression of photogenerated electron–hole recombination,[15,34,37] which can be attributed to the formation of well-developed heterojunction interfaces between BiOI and BiOBr,[33] and result in the significant enhancement of the composites' photocatalytic activities.

Among the as-prepared composites, 0.6BiOI/0.4BiOBr was identified as the most effective photocatalyst, achieving over 90% IC degradation. In contrast, the lower photocatalytic activity of 0.8BiOI/0.2BiOBr composite, despite its slightly

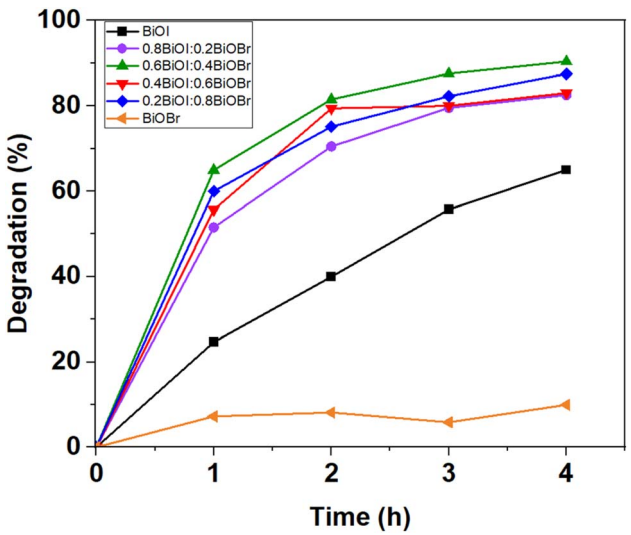

Fig. 7 IC photodegradation under visible light irradiation over the synthesized materials.

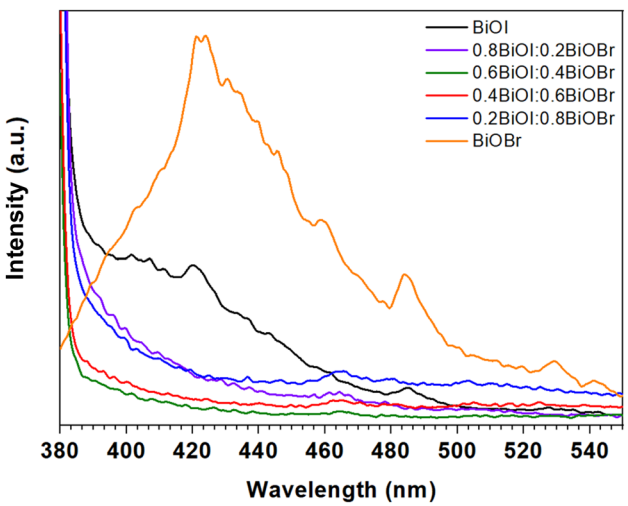

Fig. 8 PL spectra of the synthesized materials.

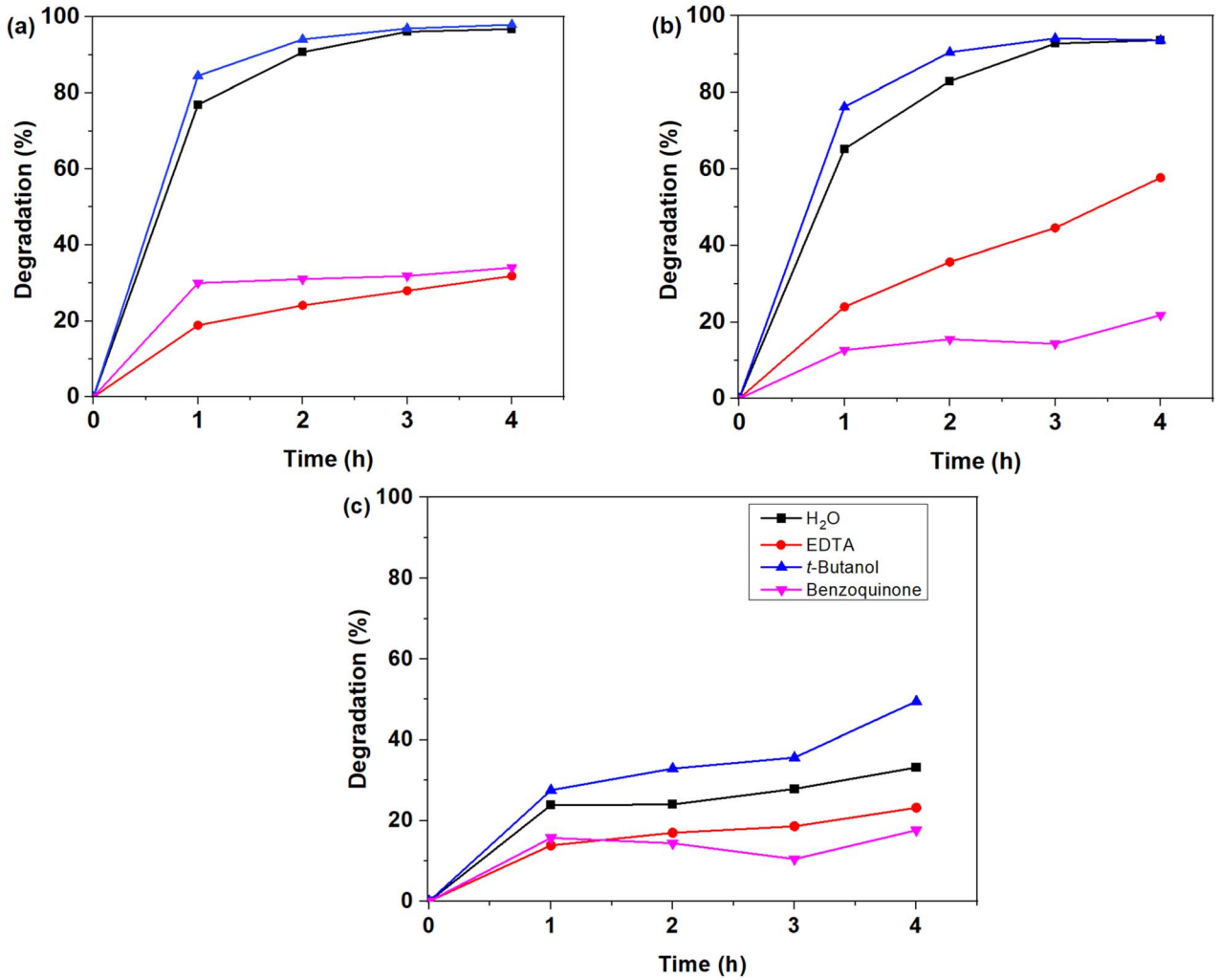

Fig. 9 The effects of different scavengers for the IC photodegradation efficiencies of 0.6BiOI/0.4BiOBr composite (a), BiOI (b), and BiOBr (c).

narrower band gap (2.21 *vs.* 2.25 eV), can be rationalized by its higher PL intensity (Fig. 8), indicating enhanced recombination rate of photogenerated carriers. Furthermore, SEM analysis (Fig. 3) revealed that the 0.6BiOI/0.4BiOBr composite exhibited relatively smaller and more uniformly distributed structures compared to 0.8BiOI/0.2BiOBr. This morphology provides a higher effective surface area and promotes more intimate interfacial contact between BiOI and BiOBr, facilitating efficient heterojunction formation and charge transfer. In contrast, the excess BiOI in 0.8BiOI/0.2BiOBr composite likely leads to aggregation and reduced heterojunction interface, thereby limiting charge separation efficiency.[15] Conversely, 0.6BiOI/0.4BiOBr composite achieved a more balanced composition that maximizes heterojunction interfaces, enabling superior charge separation and higher photocatalytic activity, even with a slightly wider band gap. These results indicated that photocatalytic activity in this system (0.6BiOI/0.4BiOBr) is governed primarily by charge separation efficiency and interfacial properties rather than band gap variation alone. Altogether, 0.6BiOI/0.4BiOBr composite was confirmed as the finest photocatalyst for IC photodegradation, and was further introduced to scavenger experiments to verify the possible mechanisms.

3.3. Proposed mechanisms

The mechanism in the removal of IC dye was proposed based on the alteration in the efficiencies of BiOI, BiOBr, and 0.6BiOI/0.4BiOBr composite with the addition of three radical scavengers, including BQ, EDTA, and *t*-butanol during the photodegradation processes. These scavengers were respectively deployed to trap superoxide radicals ($^{\bullet}O_2^-$), h^+, and $^{\bullet}OH$, which are prominent reactive oxygen species in photocatalytic oxidation reactions.[38] As illustrated in Fig. 9a, the degradation of IC dye by means of 0.6BiOI/0.4BiOBr composite were significantly attenuated as BQ and EDTA were introduced, while the addition of *t*-butanol, on the other hand, displayed the negligible effect on the degradation rate. These data, together with the significant resemblance found in the similar analyses of BiOI (Fig. 9b) and BiOBr (Fig. 9c), suggested the superior roles of $^{\bullet}O_2^-$ radicals and photo-induced holes h^+ over $^{\bullet}OH$ radicals in photodegradation of IC dye using the composite, which were relevant to the studies of Lin *et al.*[38] and Arana-Trenado *et al.*[28]

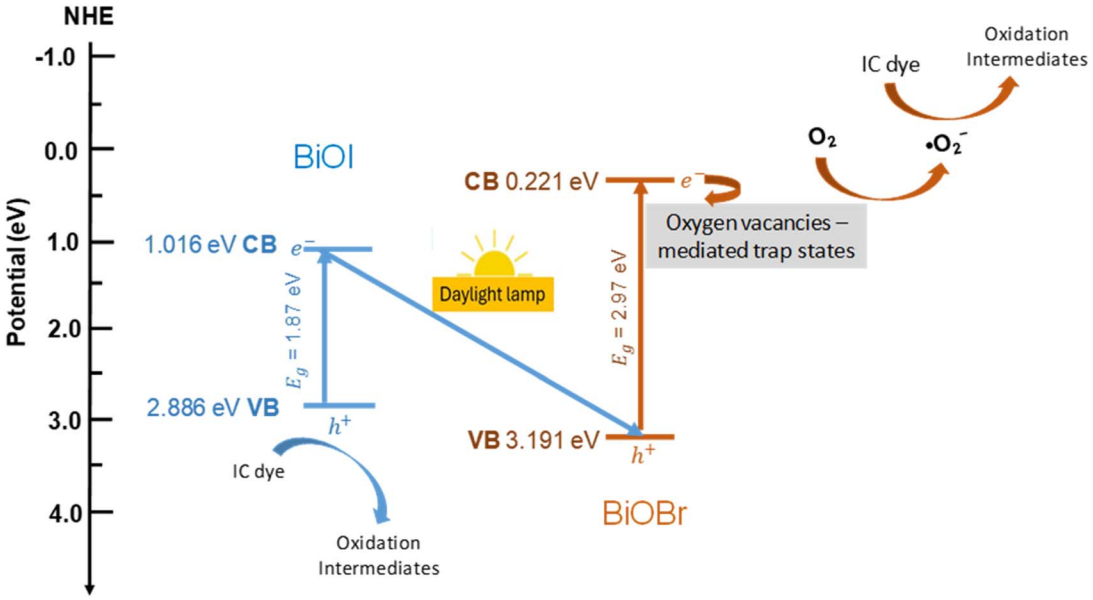

Fig. 10 Schematic illustration of a heterojunction-mediated and oxygen vacancy-assisted charge separation mechanism for the enhanced photocatalytic performance of the BiOI/BiOBr composites.

Further analysis on the band structure diagram of 0.6BiOI/0.4BiOBr composite, presented in Fig. 10, was conducted for more valid information in the material's visible light photocatalytic mechanism. Based on Mulliken electronegativity theory for atoms, the valence band (VB) and conduction band (CB) potentials, E_{VB} and E_{CB} respectively, of BiOI and BiOBr components in the heterojunction composite were estimated by eqn (2) and (3), in which X is the electronegativity of the semiconductor, and E^e is the standard electrode potential on the hydrogen scale (at around 4.5 eV).[15,38]

$$E_{VB} = X - E^e + 0.5\,E_g \quad (2)$$

$$E_{CB} = E_{VB} - E_g \quad (3)$$

The VB and CB potentials of BiOBr were estimated to be +3.191 eV and +0.221 eV, respectively, while those of BiOI were +2.886 eV and +1.016 eV. In accordance with the obtained data, the possible mechanism in IC dye photocatalytic degradation by the prepared 0.6BiOI/0.4BiOBr composite was demonstrated in Fig. 10. Under visible-light irradiation, photons with energy equal to or greater than the band gaps of BiOI (1.87 eV) and BiOBr (2.97 eV) are absorbed by the composite, leading to the excitation of electrons from the VB to the CB and the formation of electron–hole pairs (e^-/h^+) (R1). As the initial CB potential of BiOI (+1.016 eV) is more positive than that of BiOBr (+0.221 eV), the migration of photogenerated electrons from the CB of BiOI to the CB of BiOBr was unfavorable. Instead, an internal electric field-driven charge recombination pathway is favored: electrons in the CB of BiOI recombine with holes in the VB of BiOBr at the heterojunction interface, as also proposed by Zhang *et al.*[39] This process preserves the relatively more reducing electrons in the more negative CB of BiOBr and the relatively more oxidizing holes in the more positive VB of BiOI, thereby suppressing bulk recombination. Nevertheless, the standard reduction potential of $O_2/{}^{\bullet}O_2^-$ is −0.33 eV *vs.* NHE,[40] while the CB potential of BiOBr is +0.221 eV – more positive than this threshold. This indicates that the generation of ${}^{\bullet}O_2^-$ cannot be rationalized by a conventional band-to-band electron transfer mechanism alone, suggesting the involvement of additional interfacial effects. In this context, surface oxygen vacancies (OVs), which are commonly reported in bismuth oxyhalides, play a decisive role in molecular oxygen activation. As demonstrated in detailed studies on BiOCl,[41] OVs introduce localized electronic states (mid-gap defect states composed of Bi 6p orbitals) lying just below the CB minimum. These defect states act as shallow electron traps. The localized electrons trapped at OV sites can be directly back-transferred to the adsorbed O_2 molecules through a surface-mediated electron transfer process, generating ${}^{\bullet}O_2^-$ (R2). Meanwhile, the photogenerated holes at BiOI may participate in oxidation reactions directly at the catalyst surface (R3). These reactive species subsequently promote the degradation of IC dye into smaller products (R4). Accordingly, the generation of reactive species and the subsequent degradation of IC dye can be described by the following reactions:

$$\text{BiOI/BiOBr} + h\nu \rightarrow e^- \text{ (CB)} + h^+ \text{ (VB)} \quad \text{(R1)}$$

$$O_2 \text{ (ads)} + e^- \text{ (trapped at OV)} \rightarrow {}^{\bullet}O_2^- \quad \text{(R2)}$$

$$\text{IC dyes} + h^+ \rightarrow \text{oxidation intermediates} \quad \text{(R3)}$$

$$\text{IC dyes} + h^+ + {}^{\bullet}O_2^- \rightarrow \text{degradation products} \quad \text{(R4)}$$

Overall, the enhanced photocatalytic activity is attributed to heterojunction-mediated charge separation and oxygen vacancy-assisted charge transfer.

4. Conclusions

Herein, BiOI/BiOBr composites with varying mmol ratios of BiOI and BiOBr were successfully prepared *via* a facile modified deposition–precipitation method. Comprehensive analysis on the composites' morphology, crystalline phase, elemental composition and optical property characterized them as visible light responsive photocatalysts whose heterojunction interfaces between BiOI and BiOBr efficiently contributed to the separation of photogenerated electron–hole pairs and enhanced the photocatalytic activity. Evaluation on these materials' feasibility in IC dye photodegradation confirmed the superior enhancement in their visible-light-irradiated photocatalysis in comparison with the pure BiOI and BiOBr. The 0.6BiOI/0.4BiOBr composite was demonstrated as the most effective photocatalyst for IC dye degradation in which $^{\bullet}O_2^-$ radicals and photo-induced holes h^+ were consolidated as the determinant reactive species in the composite photocatalysis. These positive data have indicated the potential of Bismuth-based oxyhalides heterojunction composites as effective photocatalysts for the treatment of IC dyes. While the current photocatalytic analysis is primarily based on UV-vis absorbance changes, which mainly reflect decolorization of the dye, the involvement of reactive species ($^{\bullet}O_2^-$ and h^+) indicates that oxidative degradation of indigo carmine likely occurs. However, UV-vis spectroscopy alone cannot fully distinguish between partial degradation and complete mineralization. Therefore, further studies using complementary techniques, such as total organic carbon (TOC) analysis or liquid chromatography-mass spectrometry (LC-MS), are recommended to elucidate the complete mineralization pathway.

Author contributions

Cheewita Suwanchawalit: investigation, data curation, writing – original draft, writing – review & editing. Soontorn Suvokhiaw: data curation, writing – review & editing. Montri Aiempanakit: data curation, writing – review & editing. Hoang-Vinh-Truong Phan, Van-Kieu Nguyen: methodology, writing – original draft. Le-Thuy-Thuy-Trang Hoang: conceptualization, project administration, writing – review & editing.

Conflicts of interest

The authors report there are no conflict of interests to declare.

Data availability

The data used to support the findings of this study are included within the article.

Acknowledgements

We acknowledge Nguyen Tat Thanh University, Ho Chi Minh City, Vietnam for supporting this study.

References

1 T. Shindhal, P. Rakholiya, S. Varjani, A. Pandey, H. H. Ngo, W. Guo, H. Y. Ng and M. J. Taherzadeh, *Bioengineered*, 2021, **12**, 70–87, DOI: 10.1080/21655979.2020.1863034.
2 R. Rehman and S. Majeed, *Int. J. Phytorem.*, 2022, **24**, 1004–1013, DOI: 10.1080/15226514.2021.1991269.
3 M. F. Chowdhury, S. Khandaker, F. Sarker, A. Islam, M. T. Rahman and M. R. Awual, *J. Mol. Liq.*, 2020, **318**, 114061, DOI: 10.1016/j.molliq.2020.114061.
4 J. Trujillo-Reyes, V. Sánchez-Mendieta, A. Colín-Cruz and R. A. Morales-Luckie, *Water, Air, Soil Pollut.*, 2010, **207**, 307–317, DOI: 10.1007/s11270-009-0138-1.
5 J. A. Rauh-Hain and M. R. Laufer, *Fertil. Steril.*, 2011, **95**, 1113–1114, DOI: 10.1016/j.fertnstert.2010.12.017.
6 A. Mittal, J. Mittal and L. Kurup, *J. Environ. Prot. Sci.*, 2007, **1**, 92–100.
7 R. L. Metcalf, *Ullmann's Encycl. Ind. Chem.*, 2000, **13837329**, 264–322.
8 V. Katheresan, J. Kansedo and S. Y. Lau, *J. Environ. Chem. Eng.*, 2018, **6**(4), 4676–4697, DOI: 10.1016/j.jece.2018.06.060.
9 J. Naitoh and B. M. Fox, *Urology*, 1994, **44**(2), 271–272, DOI: 10.1016/S0090-4295(94)80149-5.
10 M.-E. Ristea and O. Zarnescu, *J. Xenobiot.*, 2023, **13**(3), 509–528, DOI: 10.3390/jox13030033.
11 J. Zhang, P. Zhang, S. Zhang and Q. Zhou, *Sep. Sci. Technol.*, 2014, **49**(6), 877–886, DOI: 10.1080/01496395.2013.863340.
12 A. P. Chowdhury and B. H. Shambharkar, *Asia-Pac. J. Chem. Eng.*, 2018, **13**(3), e2182, DOI: 10.1002/apj.2182.
13 M. Arumugam and M. Y. Choi, *J. Ind. Eng. Chem.*, 2020, **81**, 237–268, DOI: 10.1016/j.jiec.2019.09.013.
14 S. Sood, S. Kumar, A. Umar, A. Kaur, S. K. Mehta and S. K. Kansal, *J. Alloys Compd.*, 2015, **650**, 193–198, DOI: 10.1016/j.jallcom.2015.07.164.
15 J. Cao, B. Xu, B. Luo, H. Lin and S. Chen, *Catal. Commun.*, 2011, **13**(1), 63–68, DOI: 10.1016/j.catcom.2011.06.019.
16 M. R. Elamin, K. H. Ibnaouf, N. Y. Elamin, F. A. Adam, A. H. Alolayan and B. Y. Abdulkhair, *Inorganics*, 2022, **10**(5), 65–78, DOI: 10.3390/inorganics10050065.
17 L. Meng, Y. Qu and L. Jing, *Chin. Chem. Lett.*, 2021, **32**(11), 3265–3276, DOI: 10.1016/j.cclet.2021.03.083.
18 X. Wang, H. Liang, X. Zhao, X. Fan and J. Bai, *Mater. Today Sustain.*, 2024, **27**, 100909, DOI: 10.1016/j.mtsust.2024.100909.
19 P. Intaphong, A. Phuruangrat, S. Thongtem and T. Thongtem, *Mater. Lett.*, 2018, **213**, 88–91, DOI: 10.1016/j.matlet.2017.11.014.
20 H. Cheng, B. Huang, Y. Dai, X. Qin and X. Zhang, *Langmuir*, 2010, **26**(9), 6618–6624, DOI: 10.1021/la903943s.
21 S. Balu, D. Ganapathy, S. Arya, A. Raij and A. K. Sundramoorthy, *RSC Adv.*, 2024, **14**, 14392–14424, DOI: 10.1039/d4ra01307g.
22 M.-Y. Heng, H.-L. Shao, J.-T. Sun, Q. Huang, S.-L. Shen, G.-Z. Yang, Y.-H. Xue and S.-N. Xiao, *Rare Met.*, 2025, **44**(2), 1108–1121, DOI: 10.1007/s12598-024-03000-4.

23 P. Zhang, H. Liu, H. Liang, J. Bai and C. Li, *Chem. Res. Chin. Univ.*, 2020, **36**, 1227–1233, DOI: 10.1007/s40242-020-0170-7.
24 M. Lu, X. Xiao and G. Zeng, *J. Alloys Compd.*, 2021, **885**, 160996, DOI: 10.1016/j.jallcom.2021.160996.
25 N. Zhang and D. Chu, *J. Nanopart. Res.*, 2020, **22**, 206–215, DOI: 10.1007/s11051-020-04938-z.
26 D. Dai, J. Qiu, G. Xia, L. Zhang, H. Ma, L. Yang and J. Yao, *Int. J. Biol. Macromol.*, 2023, **227**, 1317–1324, DOI: 10.1016/j.ijbiomac.2022.12.007.
27 H. Liu, C. Yang, J. Huang, J. Chen, J. Zhong and J. Li, *Inorg. Chem. Commun.*, 2020, **113**, 107806, DOI: 10.1016/j.inoche.2020.107806.
28 J. A. Arana-Trenado, D. Ramírez-Ortega, A. Serrano-Lázaro, A. Hernández-Gordillo, S. E. Rodil and M. Bizarro, *Dalton Trans.*, 2022, **51**, 2413–2427, DOI: 10.1039/D1DT03782J.
29 R. Bibi, Q. Shen, L. Wei, D. Hao, N. Li and J. Zhou, *RSC Adv.*, 2018, **8**, 2048–2058, DOI: 10.1039/C7RA11500H.
30 L. Yosefi, M. Haghighi and S. Minaei, *Mater. Today Sustain.*, 2024, **26**, 100723, DOI: 10.1016/j.mtsust.2024.100723.
31 S. Vahabirad and A. Nezamzadeh-Ejhieh, *J. Solid State Chem.*, 2022, **310**, 123018, DOI: 10.1016/j.jssc.2022.123018.
32 S. S. Imam, R. Adnan, N. H. Mohd Kaus and M. H. Hussin, *J. Mater. Sci.:Mater. Electron.*, 2019, **30**, 6263–6276, DOI: 10.1007/s10854-019-00930-z.
33 Y. Liu, J. Xu, L. Wang, H. Zhang, P. Xu, X. Duan, H. Sun and S. Wang, *Nanomaterials*, 2017, **7**(3), 64–82, DOI: 10.3390/nano7030064.
34 J. Zhang, Z. Chen, Y. Qiu, M. Li, H. Yang, Y. Huang and J. Chen, *Inorg. Chem. Commun.*, 2018, **98**, 58–61, DOI: 10.1016/j.inoche.2018.09.027.
35 Y. Wang, K. Deng and L. Zhang, *J. Phys. Chem. C*, 2011, **115**(29), 14300–14308, DOI: 10.1021/jp2042069.
36 J. Ding, G. Su, Y. Zhou, H. Yin, S. Wang, J. Wang and W. Zhang, *Environ. Pollut.*, 2024, **341**, 122942, DOI: 10.1016/j.envpol.2023.122942.
37 K. Gao, H. Zhu, C. Zhang, X. Song, L. Lao, L. Ni, J. Chen, C. Cheng and X. Wang, *Sol. RRL*, 2022, **6**(12), 2200869, DOI: 10.1002/solr.2022Wee00869.
38 L. Lin, M. Huang, L. Long, Z. Sun, W. Zheng and D. Chen, *Ceram. Int.*, 2014, **40**, 11493–11501, DOI: 10.1016/j.ceramint.2014.03.039.
39 S. Zhang, J. Guo, S. Deng, R. Zhang, Q. Zhu, Y. Liu, X. Lin and Y. Li, *J. Environ. Chem. Eng.*, 2024, **12**(3), 113017, DOI: 10.1016/j.jece.2024.113017.
40 Y. A. Ilan, G. Czapski and D. Meisel, *Biochim. Biophys. Acta, Bioenerg.*, 1976, **430**(2), 209–224, DOI: 10.1016/0005-2728(76)90080-3.
41 H. Li, J. Li, Z. Ai, F. Jia and L. Zhang, *Angew. Chem., Int. Ed.*, 2017, **57**(1), 122–138, DOI: 10.1002/anie.201705628.